Implementation of the marchenko method

Thorbecke, Jan; Slob, Evert; Brackenhoff, Joeri; van der Neut, Joost; Wapenaar, Kees

DOI
10.1190/GEO2017-0108.1

Publication date
2017

Document Version
Final published version

Published in
Geophysics

GEOPHYSICS, VOL. 82, NO. 6 (NOVEMBER-DECEMBER 2017); P. WB29–WB45, 12 FIGS., 1 TABLE.
10.1190/GEO2017-0108.1

Implementation of the Marchenko method

Jan Thorbecke[1], Evert Slob[1], Joeri Brackenhoff[1], Joost van der Neut[1], and Kees Wapenaar[1]

ABSTRACT

The Marchenko method makes it possible to compute subsurface-to-surface Green's functions from reflection measurements at the surface. Applications of the Marchenko method have already been discussed in many papers, but its implementation aspects have not yet been discussed in detail. Solving the Marchenko equation is an inverse problem. The Marchenko method computes a solution of the Marchenko equation by an (adaptive) iterative scheme or by a direct inversion. We have evaluated the iterative implementation based on a Neumann series, which is considered to be the conventional scheme. At each iteration of this scheme, a convolution in time and an integration in space are performed between a so-called focusing (update) function and the reflection response. In addition, by applying a time window, one obtains an update, which becomes the input for the next iteration. In each iteration, upgoing and downgoing focusing functions are updated with these terms. After convergence of the scheme, the resulting upgoing and downgoing focusing functions are used to compute the upgoing and downgoing Green's functions with a virtual-source position in the subsurface and receivers at the surface. We have evaluated this algorithm in detail and developed an implementation that reproduces our examples. The software fits into the Seismic Unix software suite of the Colorado School of Mines.

INTRODUCTION

The Marchenko method relates Green's function from a virtual source inside a medium to the reflection response at the surface of that medium. The method has been introduced to the geophysical world by Broggini and Snieder (2012). In close collaboration with these authors, their work is extended to 2D and 3D media by Broggini et al. (2012) and Wapenaar et al. (2013). Based on the outputs of the Marchenko method, upgoing and downgoing Green's functions can be estimated, for any point in the subsurface to the surface array, using the reflection response recorded at the surface. The Green's function is the earth impulse response and is fundamental in many processing schemes.

The application of the results of the Marchenko method is therefore manifold: It has been used for imaging the subsurface without the disturbing effect of internal multiples (Behura et al., 2014; Slob et al., 2014; Wapenaar et al., 2014b; da Costa Filho et al., 2015; van der Neut et al., 2015c; Vasconcelos et al., 2015; Meles et al., 2016; Ravasi et al., 2016), internal multiple elimination in the data domain (Meles et al., 2015; van der Neut and Wapenaar 2016; da Costa Filho et al., 2017), and retrieving the homogeneous Green's function between any two points inside a medium from the reflection response (Wapenaar et al., 2017).

In the first geophysical Marchenko papers, the computation of the Green's function is based on iteratively updating acoustic pressure fields (Wapenaar et al., 2013). This pressure-based algorithm requires two separate iterative updates to calculate the upgoing or downgoing Green's functions at a virtual source position. Slob et al. (2014) combine these separate iterative schemes into one. In this combined scheme, upgoing and downgoing focusing functions are updated in each iteration. Wapenaar and Slob (2014) and da Costa Filho et al. (2014) extend the method to elastic media, Singh et al. (2015) include the free-surface multiples, and Slob (2016) adapts the method to dissipative acoustic media. Apart from iterative schemes, the Marchenko method can also be implemented as an adaptive subtraction (Staring et al., 2016) or a least-squares inversion (van der Neut et al., 2015b; Slob and Wapenaar, 2017).

In this paper, we describe in detail the implementational aspects of the 2D iterative acoustic-Marchenko method based on focusing functions. Although the algorithm is straightforward to implement, the treatment of amplitudes and the initialization steps of the first iterations require special attention. The input of the method is a

Peer-reviewed code related to this article can be found at http://software.seg.org/2017/0007.
Manuscript received by the Editor 17 February 2017; revised manuscript received 8 June 2017; published ahead of production 21 July 2017; published online 06 September 2017.
[1]Delft University of Technology, Department of Geoscience and Engineering, GA Delft, Delft, The Netherlands. E-mail: j.w.thorbecke@tudelft.nl; e.c.slob@tudelft.nl; j.a.brackenhoff@tudelft.nl; j.r.vanderneut@tudelft.nl; c.p.a.wapenaar@tudelft.nl.

reflection response without free-surface multiples, and it is deconvolved by its source wavelet. The output of a surface-related multiple elimination (SRME) scheme can (in principle) provide this reflection response. A (smooth) background model is needed to calculate an initial focusing function to start the algorithm. The "Numerical examples" section demonstrates the use of the algorithm and provides a user's first steps with the Marchenko technique.

The software bundled with this paper contains all source code and scripts to reproduce the examples presents herein. The code can also be found at its GitHub repository (Thorbecke, 2017). The GitHub repository contains the most up-to-date stable version with bug fixes and the latest developments. In Appendix A, the input parameters of the programs are explained. To reproduce the figures in this manuscript and to carry out a few post- and preprocessing steps, Seismic Unix (SU) (Cohen and Stockwell, 2016) is required.

MARCHENKO METHOD

The Marchenko method is briefly introduced here, aiming at an explanation of the method that helps to understand the algorithm. The references mentioned in the "Introduction" section provide additional details on the derivation of this method. In an imagined medium truncated below level z_i, we introduce a focusing function f_1. The truncated medium is identical to the actual medium above depth level z_i and is reflection free below this depth level. As illustrated in Figure 1, the actual and truncated media are reflection free above the surface boundary $\partial\mathbb{D}_0$. We also introduce upgoing and downgoing parts of the f_1 focusing function (Slob et al., 2014):

$$f_1(\mathbf{x},\mathbf{x}_F,t) = f_1^+(\mathbf{x},\mathbf{x}_F,t) + f_1^-(\mathbf{x},\mathbf{x}_F,t), \tag{1}$$

where $\mathbf{x}_F = (x_F, z_i)$ is a focal position on the boundary $\partial\mathbb{D}_i$, $\mathbf{x}$ is an observation point in the medium, and t is the time (see Figure 1). In our notation, the first argument represents the receiver location and the second argument stands for the focal point. The superscript "+" in f_1^+ denotes a downgoing field at observation point $\mathbf{x}$, and the superscript "−" in f_1^- denotes an upgoing field, also at $\mathbf{x}$. Below

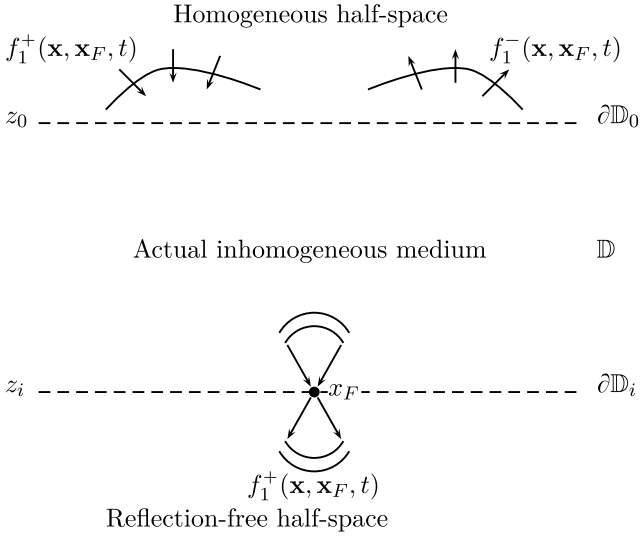

Figure 1. Downgoing and upgoing components of the focusing function f_1 for the 2D wave equation in a truncated medium.

boundary $\partial\mathbb{D}_i$ only f_1^+ continues as a diverging downgoing field into the reflection-free half-space.

The $f_1^\pm$ focusing functions are defined to relate the upgoing and downgoing Green's functions in the actual medium with the reflection response at the surface (Wapenaar et al., 2014b):

$$G^+(\mathbf{x}_F,\mathbf{x}_R,t) = -\int_{\partial\mathbb{D}_0}\int_{t'=-\infty}^{t} R(\mathbf{x}_R,\mathbf{x},t-t')f_1^-(\mathbf{x},\mathbf{x}_F,-t')\mathrm{d}t'\mathrm{d}\mathbf{x} + f_1^+(\mathbf{x}_R,\mathbf{x}_F,-t), \tag{2}$$

$$G^-(\mathbf{x}_F,\mathbf{x}_R,t) = \int_{\partial\mathbb{D}_0}\int_{t'=-\infty}^{t} R(\mathbf{x}_R,\mathbf{x},t-t')f_1^+(\mathbf{x},\mathbf{x}_F,t')\mathrm{d}t'\mathrm{d}\mathbf{x} - f_1^-(\mathbf{x}_R,\mathbf{x}_F,t), \tag{3}$$

where $R(\mathbf{x}_R,\mathbf{x},t)$ is the reflection response after surface multiple elimination, deghosting, and deconvolution of the wavelet. The first argument in R represents the receiver location, the second argument represents the source location, and the last argument is the time. The function R is a scaled (factor −2) pressure wavefield at $\mathbf{x}_R$ of a vertical force source F_z at $\mathbf{x}$ or, via reciprocity, the particle velocity field V_z at $\mathbf{x}$ of a point source of the volume injection rate at $\mathbf{x}_R$ (Wapenaar et al., 2012). This reflection response is related to a Green's function by

$$\frac{\partial R(\mathbf{x}_R,\mathbf{x},t)}{\partial t} = \frac{2}{\rho(\mathbf{x})}\frac{\partial G^s(\mathbf{x}_R,\mathbf{x},t)}{\partial z}, \tag{4}$$

with G^s the Green's function of the scattered field only (it does not contain the direct field). The upper integration boundary $t' = t$ of the time integral in equations 2 and 3 accounts for the causality of the reflection response $R(\mathbf{x}_R,\mathbf{x},t-t')$. Summing equations 2 and 3 and using source-receiver reciprocity for Green's function gives (Wapenaar et al., 2017)

$$G(\mathbf{x}_R,\mathbf{x}_F,t) = \int_{\partial\mathbb{D}_0}\int_{t'=-\infty}^{t} R(\mathbf{x}_R,\mathbf{x},t-t')f_2(\mathbf{x}_F,\mathbf{x},t')\mathrm{d}t'\mathrm{d}\mathbf{x} + f_2(\mathbf{x}_F,\mathbf{x}_R,-t), \tag{5}$$

where the Green's function $G(\mathbf{x}_R,\mathbf{x}_F,t)$ represents the response to a virtual point source of volume injection rate at $\mathbf{x}_F$ and pressure receivers at the surface $\mathbf{x}_R$. The focusing function f_2 is defined as

$$f_2(\mathbf{x}_F,\mathbf{x},t) = f_1^+(\mathbf{x},\mathbf{x}_F,t) - f_1^-(\mathbf{x},\mathbf{x}_F,-t). \tag{6}$$

Wapenaar et al. (2014b) introduce $f_2(\mathbf{x}_F,\mathbf{x},t)$ as a focusing function that has its focal plane at $\partial\mathbb{D}_0$. Here, we merely use f_2 as a compact notation for the combination of the one-way focusing functions f_1^+ and f_1^-, as defined in equation 6. Note that the time-reversed upgoing function f_1^- can be interpreted as a downgoing function, similar to f_1^+. Hence, from here onward, we interpret $f_2(\mathbf{x}_F,\mathbf{x},t)$ as a downgoing focusing function that is emitted into the medium from $\mathbf{x}$ and that focuses at receiver location $\mathbf{x}_F$. The argument change in equation 6 between $\mathbf{x}$ and $\mathbf{x}_F$ in the left side f_2 and the right side $f_1^\pm$ follows from the same logic in the order of the arguments as defined by Wapenaar et al. (2014b). In the "Numerical examples" section, we demonstrate that f_2 can be back-propagated into the medium and focuses at $\mathbf{x}_F$. In Wapenaar

et al. (2013), a (reciprocal) relation between $f_2(\mathbf{x}_F, \mathbf{x}, t)$ and a downgoing wavefield $p^+(\mathbf{x}, \mathbf{x}_F, t)$ is given. Together with p^+ there is also a p^- defined, the upgoing reflection response at $\mathbf{x}$ from the focal point at $\mathbf{x}_F$. The sum of p^+ and p^- gives also the Green's function of equation 5. The $p^\pm$ functions are just a different notation of the Marchenko method and can be used to compute the Green's functions in a convenient way. These $p^\pm$ functions are therefore used in the implementation to compute the Green's function. From an educational point of view, the Marchenko method is more easily understood using the focusing functions only, and we will continue along that way.

The above equations, on which the following implementation is based on, use pressure-normalized fields. Other papers derive similar equations based on flux-normalized fields (Wapenaar et al., 2014a; Singh et al., 2015; van der Neut et al., 2015b). The relationship between pressure- and flux-normalized representations is explained by Wapenaar et al. (2014a).

The Marchenko algorithm estimates focusing functions $f_1^+(\mathbf{x}, \mathbf{x}_F, t)$ and $f_1^-(\mathbf{x}, \mathbf{x}_F, t)$. However, equations 2 and 3 are by themselves insufficient to determine f_1; there are four unknowns, but only two equations. We can eliminate two unknowns by exploiting the fact that the focusing functions and Green's functions have different causality properties in the time-space domain. Based on the principle of causality, we know that no energy arrives before the first arrival $t_d(\mathbf{x}_R, \mathbf{x}_F)$; hence, the Green's function $G(\mathbf{x}_R, \mathbf{x}_F, t < t_d(\mathbf{x}_R, \mathbf{x}_F))$ is zero. This also holds for the upgoing and downgoing Green's functions and leads to

$$0 = -\int_{\partial\mathbb{D}_0}\int_{t'=-\infty}^{t} R(\mathbf{x}_R, \mathbf{x}, t-t') f_1^-(\mathbf{x}, \mathbf{x}_F, -t')\mathrm{d}t'\mathrm{d}\mathbf{x} + f_1^+(\mathbf{x}_R, \mathbf{x}_F, -t), \tag{7}$$

$$0 = \int_{\partial\mathbb{D}_0}\int_{t'=-\infty}^{t} R(\mathbf{x}_R, \mathbf{x}, t-t') f_1^+(\mathbf{x}, \mathbf{x}_F, t')\mathrm{d}t'\mathrm{d}\mathbf{x} - f_1^-(\mathbf{x}_R, \mathbf{x}_F, t), \tag{8}$$

where $t < t_d(\mathbf{x}_R, \mathbf{x}_F)$ in both equations above.

The combination of equations 7 and 8 is known as the Marchenko equation. These equations form the basis of the iterative scheme, which estimates focusing functions f_1^+ and f_1^-. In Wapenaar et al. (2014a), the relation

$$f_1^+(\mathbf{x}, \mathbf{x}_F, t) = T^{\mathrm{inv}}(\mathbf{x}_F, \mathbf{x}, t) \tag{9}$$

is used to derive an initial estimate for f_1^+ that can start the inversion scheme. In equation 9, $T^{\mathrm{inv}}(\mathbf{x}_F, \mathbf{x}, t)$ is the inverse of the transmission response of the truncated medium, which is equal to the actual medium between $\partial\mathbb{D}_0$ and $\partial\mathbb{D}_i$, for a source at $\mathbf{x}$ (at $\partial\mathbb{D}_0$) and a receiver at $\partial\mathbb{D}_i$. It is assumed that this inverse transmission response T^{inv} can be composed as a direct wave followed by scattering coda (van der Neut et al., 2015b):

$$f_1^+(\mathbf{x}, \mathbf{x}_F, t) = T_d^{\mathrm{inv}}(\mathbf{x}_F, \mathbf{x}, t) + M^+(\mathbf{x}, \mathbf{x}_F, t), \tag{10}$$

where M^+ is the unknown scattering coda and T_d^{inv} is the direct arrival of the inverse transmission response. In equation 10, the inverse of the direct arrival of the transmission response is needed. For simplicity, we take the time reversal of the direct arrival of Green's function; $G_d(\mathbf{x}, \mathbf{x}_F, -t)$:

$$f_1^+(\mathbf{x}, \mathbf{x}_F, t) \approx G_d(\mathbf{x}, \mathbf{x}_F, -t) + M^+(\mathbf{x}, \mathbf{x}_F, t). \tag{11}$$

We thereby introduce an overall scaling error and an offset-dependent amplitude error, proportional to transmission losses, in the final result. The function $G_d(\mathbf{x}, \mathbf{x}_F, -t)$ is the time-reversed direct arrival part of the transmission response to subsurface focal point $\mathbf{x}_F$ and can, for example, be computed from a smooth macromodel. As mentioned before, the arrival time of $G_d(\mathbf{x}, \mathbf{x}_F, t)$ is t_d; hence, $G_d(\mathbf{x}, \mathbf{x}_F, t)$ is zero before $t < t_d$. The multiple scattering coda $M^+(\mathbf{x}, \mathbf{x}_F, t)$ follows after the first arrival of f_1^+, and it is zero for $t \le -t_d$. It can also be shown that it is also zero for $t \ge +t_d$ (Slob et al., 2014).

Equations 7 and 8 are only valid for $t < t_d$. Therefore, we define a time-window function:

$$\theta(\mathbf{x}_R, \mathbf{x}_F, t) = \begin{cases} 1 & t < t_d^\varepsilon \\ \frac{1}{2} & t = t_d^\varepsilon \\ 0 & t > t_d^\varepsilon \end{cases}, \tag{12}$$

where time t_d^ε is the time of the direct arrival from the focal point $\mathbf{x}_F$ to $\mathbf{x}_R$ (t_d), minus a small positive constant ε to exclude the wavelet in the direct arrival G_d. For example, a time window that sets all times $t < -t_d^\varepsilon$ to zero and applied to equation 11 mutes $G_d(-t)$, but it leaves all events of M^+ in. In the following, we will use the shorthand notation θ_t for $\theta(\mathbf{x}_R, \mathbf{x}_F, t)$. In the included Marchenko program, there is an input parameter (called `smooth`; see Appendix A for all input parameters) that defines a temporal tapering in this mute window to suppress high-frequency artifacts.

It is further assumed that it is possible to get an estimate of this direct arrival G_d of the transmission response. Given the reflection response $R(\mathbf{x}_R, \mathbf{x}, t)$ and this direct arrival $G_d(\mathbf{x}, \mathbf{x}_F, t)$ from the focal point, the Marchenko algorithm solves for the scattering coda $M^+(\mathbf{x}, \mathbf{x}_F, t)$ to estimate $f_1^+(\mathbf{x}, \mathbf{x}_F, t)$ and $f_1^-(\mathbf{x}, \mathbf{x}_F, t)$.

The iterative solution of the Marchenko equations can now be developed. The iterative scheme is started with the following initialization of M^+:

$$M_0^+(\mathbf{x}_R, \mathbf{x}_F, t) = 0. \tag{13}$$

The subscript in M_0^+ defines the iteration number. By substituting equation 11, using 13 as an initialization, into equation 8 one arrives at the initialization of f_1^-:

$$f_{1,0}^-(\mathbf{x}_R, \mathbf{x}_F, t) = \theta_t \int_{\partial\mathbb{D}_0}\int_{t'=-\infty}^{t} R(\mathbf{x}_R, \mathbf{x}, t-t') G_d(\mathbf{x}, \mathbf{x}_F, -t')\mathrm{d}t'\mathrm{d}\mathbf{x}. \tag{14}$$

Equation 14 includes the previously defined time-window function θ_t. Equations 7 and 11 are expressions for f_1^+. By combining these equations, the only part remaining in equation 11 is M^+. The iterative update of M^+ for step $k \ge 1$ is given by

$$M_k^+(\mathbf{x}_R, \mathbf{x}_F, -t) = \theta_t \int_{\partial\mathbb{D}_0}\int_{t'=-\infty}^{t} R(\mathbf{x}_R, \mathbf{x}, t-t') f_{1,k-1}^-(\mathbf{x}, \mathbf{x}_F, -t')\mathrm{d}t'\mathrm{d}\mathbf{x}. \tag{15}$$

Following the assumption in equation 11, that it is possible to write $f^+_{1,k}$ as a direct field plus scattering coda, the update at step k of $f^+_{1,k}$ is given by

$$f^+_{1,k}(\mathbf{x}_R,\mathbf{x}_F,t) = G_d(\mathbf{x}_R,\mathbf{x}_F,-t) + M^+_k(\mathbf{x}_R,\mathbf{x}_F,t). \quad (16)$$

Using equation 8 and the expression of f^+_1 in equation 16, the update of f^-_1 at step k is given by

$$f^-_{1,k}(\mathbf{x}_R,\mathbf{x}_F,t) = f^-_{1,0}(\mathbf{x}_R,\mathbf{x}_F,t) + \theta_t \int_{\partial\mathbb{D}_0}\int_{t'=-\infty}^{t} R(\mathbf{x}_R,\mathbf{x},t-t')M^+_k(\mathbf{x},\mathbf{x}_F,t')\mathrm{d}t'\mathrm{d}\mathbf{x}. \quad (17)$$

This completes the definition of the iterative Marchenko scheme. In the next section, the first few iterations are discussed in detail and illustrated with simple numerical examples.

MARCHENKO ALGORITHM

To compute f_1 focusing functions with the Marchenko method, two ingredients are needed:

- Reflection data without free-surface multiples, ghosts and deconvolved for the wavelet: $R(\mathbf{x}_R,\mathbf{x},t)$ with source $\mathbf{x}$ and receiver $\mathbf{x}_R$ on the same surface $\partial\mathbb{D}_0$, and small enough sampling for $\mathbf{x}_R$ and $\mathbf{x}$ to avoid spatial aliasing.
- An estimate of the direct arrival between the receiver positions at the surface ($\mathbf{x}_R$), and the focal point at $\mathbf{x}_F$: $G_d(\mathbf{x}_R,\mathbf{x}_F,t)$, and derived from it the direct arrival time $t_d(\mathbf{x}_R,\mathbf{x}_F,t)$. Note that t_d can also be computed by another method, for example, an eikonal solver.

Given these two components, the iterative method can be initialized and the iterations of the Marchenko method can start.

The first few iterations

The initialization of the method is given in equations 13 and 14. The time-windowed expression for $f^-_{1,0}(\mathbf{x}_R,\mathbf{x}_F,t)$ in equation 14 is renamed to

$$-N_0(\mathbf{x}_R,\mathbf{x}_F,-t) = \theta_t \int_{\partial\mathbb{D}_0}\int_{t'} R(\mathbf{x}_R,\mathbf{x},t-t')G_d(\mathbf{x},\mathbf{x}_F,-t')\mathrm{d}t'\mathrm{d}\mathbf{x}. \quad (18)$$

At each iteration, the spatial integration and temporal convolution with R plays an important role because it is used to define new focusing updates given by terms N_i (see also appendix B of Wapenaar et al., 2014b). These N_i terms are used to update the estimates of the focusing functions f^+_1 and f^-_1. Although the N_i terms are not strictly needed to describe the method, they are introduced here to remain as close as possible to the actual implementation.

For computational efficiency, the temporal convolution of R is implemented in the Fourier domain. The spatial integration is carried out by summing the resulting traces of the time convolution over a common-receiver gather. The introduced time-window sets events for $t > t^e_d$ to zero, in accordance with equation 18. Applying the mute window is therefore a crucial and mandatory step in the Marchenko method; without it, the method would be incorrect.

Given these initializations, the first step in the algorithm, based on equations 15–17, can be computed. This first step, $k = 1$, involves two integration-convolutions with R to update f^+_1 and f^-_1:

$$\begin{aligned} M^+_1(\mathbf{x}_R,\mathbf{x}_F,-t) &= \theta_t \int_{\partial\mathbb{D}_0}\int_{t'} R(\mathbf{x}_R,\mathbf{x},t-t')f^-_{1,0}(\mathbf{x},\mathbf{x}_F,-t')\mathrm{d}t'\mathrm{d}\mathbf{x} \\ &= -\theta_t \int_{\partial\mathbb{D}_0}\int_{t'} R(\mathbf{x}_R,\mathbf{x},t-t')N_0(\mathbf{x},\mathbf{x}_F,t')\mathrm{d}t'\mathrm{d}\mathbf{x} \\ &= N_1(\mathbf{x}_R,\mathbf{x}_F,-t), \end{aligned} \quad (19)$$

$$\begin{aligned} f^+_{1,1}(\mathbf{x}_R,\mathbf{x}_F,t) &= G_d(\mathbf{x}_R,\mathbf{x}_F,-t) + M^+_1(\mathbf{x}_R,\mathbf{x}_F,t) \\ &= G_d(\mathbf{x}_R,\mathbf{x}_F,-t) + N_1(\mathbf{x}_F,\mathbf{x}_R,t), \end{aligned} \quad (20)$$

$$\begin{aligned} f^-_{1,1}(\mathbf{x}_R,\mathbf{x}_F,t) &= f^-_{1,0}(\mathbf{x}_R,\mathbf{x}_F,t) \\ &\quad + \theta_t \int_{\partial\mathbb{D}_0}\int_{t'} R(\mathbf{x}_R,\mathbf{x},t-t')M^+_1(\mathbf{x},\mathbf{x}_F,t')\mathrm{d}t'\mathrm{d}\mathbf{x} \\ &= -N_0(\mathbf{x}_R,\mathbf{x}_F,-t) \\ &\quad + \theta_t \int_{\partial\mathbb{D}_0}\int_{t'} R(\mathbf{x}_R,\mathbf{x},t-t')N_1(\mathbf{x},\mathbf{x}_F,t')\mathrm{d}t'\mathrm{d}\mathbf{x}, \\ &= -N_0(\mathbf{x}_R,\mathbf{x}_F,-t) - N_2(\mathbf{x}_R,\mathbf{x}_F,-t), \end{aligned} \quad (21)$$

$$\begin{aligned} f_{2,1}(\mathbf{x}_F,\mathbf{x}_R,t) &= G_d(\mathbf{x}_R,\mathbf{x}_F,-t) + N_0(\mathbf{x}_R,\mathbf{x}_F,t) \\ &\quad + N_1(\mathbf{x}_R,\mathbf{x}_F,t) + N_2(\mathbf{x}_R,\mathbf{x}_F,t). \end{aligned} \quad (22)$$

The first integration-convolution with R in equation 19 is used to update f^+_1 as shown in equation 20. The second integration-convolution in equation 21 updates f^-_1. The update of f_2, introduced in equation 6, includes the results of all integration-convolutions with R.

The next step for $k = 2$ results in the following updates:

$$\begin{aligned} M^+_2(\mathbf{x}_R,\mathbf{x}_F,-t) &= \theta_t \int_{\partial\mathbb{D}_0}\int_{t'} R(\mathbf{x}_R,\mathbf{x},t-t')f^-_{1,1}(\mathbf{x},\mathbf{x}_F,-t')\mathrm{d}t'\mathrm{d}\mathbf{x} \\ &= -\theta_t \int_{\partial\mathbb{D}_0}\int_{t'} R(\mathbf{x}_R,\mathbf{x},t-t')\{N_0(\mathbf{x},\mathbf{x}_F,t) \\ &\quad + N_2(\mathbf{x},\mathbf{x}_F,t)\}\mathrm{d}t'\mathrm{d}\mathbf{x} \\ &= N_1(\mathbf{x}_R,\mathbf{x}_F,-t) + N_3(\mathbf{x}_R,\mathbf{x}_F,-t), \end{aligned} \quad (23)$$

$$\begin{aligned} f^+_{1,2}(\mathbf{x}_R,\mathbf{x}_F,t) &= G_d(\mathbf{x}_R,\mathbf{x}_F,-t) + M^+_2(\mathbf{x}_R,\mathbf{x}_F,t) \\ &= G_d(\mathbf{x}_R,\mathbf{x}_F,-t) + N_1(\mathbf{x}_R,\mathbf{x}_F,t) \\ &\quad + N_3(\mathbf{x}_R,\mathbf{x}_F,t), \end{aligned} \quad (24)$$

$$
\begin{aligned}
f_{1,2}^{-}(\mathbf{x}_R,\mathbf{x}_F,t) &= f_{1,0}^{-}(\mathbf{x}_R,\mathbf{x}_F,t) \\
&\quad + \theta_t \int_{\partial\mathbb{D}_0}\int_{t'} R(\mathbf{x}_R,\mathbf{x},t-t')M_2^{+}(\mathbf{x},\mathbf{x}_F,t')\mathrm{d}t'\mathrm{d}\mathbf{x} \\
&= -N_0(\mathbf{x}_R,\mathbf{x}_F,-t) + \theta_t \int_{\partial\mathbb{D}_0}\int_{t'} R(\mathbf{x}_R,\mathbf{x},t-t') \\
&\quad \times\{N_1(\mathbf{x},\mathbf{x}_F,t)+N_3(\mathbf{x},\mathbf{x}_F,t)\}\mathrm{d}t'\mathrm{d}\mathbf{x} \\
&= -N_0(\mathbf{x}_R,\mathbf{x}_F,-t) - N_2(\mathbf{x}_R,\mathbf{x}_F,-t) \\
&\quad - N_4(\mathbf{x}_R,\mathbf{x}_F,-t), \qquad (25)
\end{aligned}
$$

$$
\begin{aligned}
f_{2,2}(\mathbf{x}_F,\mathbf{x}_R,t) &= G_d(\mathbf{x}_R,\mathbf{x}_F,-t) + N_0(\mathbf{x}_R,\mathbf{x}_F,t) \\
&\quad + N_1(\mathbf{x}_R,\mathbf{x}_F,t) + N_2(\mathbf{x}_R,\mathbf{x}_F,t) \\
&\quad + N_3(\mathbf{x}_R,\mathbf{x}_F,t) + N_4(\mathbf{x}_R,\mathbf{x}_F,t). \qquad (26)
\end{aligned}
$$

From these updates, it becomes clear that in updating f_1^{+} in equation 24 G_d and the odd terms of N_i are used and in updating f_1^{-} in equation 25 the even terms of N_i are used. The f_2 function in equation 26 is built up from G_d and even and odd N_i terms.

In the implementation, the N_i terms are computed by

$$
N_{-1}(\mathbf{x}_R,\mathbf{x}_F,-t) = G_d(\mathbf{x},\mathbf{x}_F,-t'), \qquad (27)
$$

$$
N_i(\mathbf{x}_R,\mathbf{x}_F,-t) = -\theta_t \int_{\partial\mathbb{D}_0}\int_{t'} R(\mathbf{x}_R,\mathbf{x},t-t')N_{i-1}(\mathbf{x},\mathbf{x}_F,t')\mathrm{d}t'\mathrm{d}\mathbf{x}, \qquad (28)
$$

and are used to update the focusing functions f_1^{+}, f_1^{-}, and f_2. This makes the algorithm simple and efficient. In summary, the relations for M_m^{+}, N_i and the updates for the focusing functions for m iterations with $m \geq 1$ are

$$
M_m^{+}(\mathbf{x}_R,\mathbf{x}_F,t) = \sum_{l=0}^{m-1} N_{2l+1}(\mathbf{x}_R,\mathbf{x}_F,t), \qquad (29)
$$

$$
f_{1,m}^{+}(\mathbf{x}_R,\mathbf{x}_F,t) = G_d(\mathbf{x}_R,\mathbf{x}_F,-t) + \sum_{l=0}^{m-1} N_{2l+1}(\mathbf{x}_R,\mathbf{x}_F,t), \qquad (30)
$$

$$
f_{1,m}^{-}(\mathbf{x}_R,\mathbf{x}_F,t) = -\sum_{l=0}^{m} N_{2l}(\mathbf{x}_R,\mathbf{x}_F,-t), \qquad (31)
$$

$$
f_{2,m}(\mathbf{x}_F,\mathbf{x}_R,t) = G_d(\mathbf{x}_R,\mathbf{x}_F,-t) + \sum_{l=0}^{2m} N_l(\mathbf{x}_R,\mathbf{x}_F,t). \qquad (32)
$$

In the provided program, each computation of a focusing update term N_i is called one iteration. The implementation is shown in Algorithm 1, and a flowchart is shown in Figure 2.

The initializations of f_1^{-}, f_1^{+}, f_2, and N_i are done just before the iteration starts. The even and odd iterations for N_i update f_1^{-} and f_1^{+}, respectively. The Green's function is computed by inserting the estimate of f_2 given by equation 32 into equation 5:

$$
\begin{aligned}
G(\mathbf{x}_F,\mathbf{x}_R,t) &= f_2(\mathbf{x}_F,\mathbf{x}_R,-t) \\
&\quad + \int_{\partial\mathbb{D}_0}\int_{t'=-\infty}^{t} R(\mathbf{x}_R,\mathbf{x},t-t')G_d(\mathbf{x},\mathbf{x}_F,-t)\mathrm{d}t'\mathrm{d}\mathbf{x} \\
&\quad + \sum_{l=0}^{2m}\int_{\partial\mathbb{D}_0}\int_{t'=-\infty}^{t} R(\mathbf{x}_R,\mathbf{x},t-t')N_l(\mathbf{x},\mathbf{x}_F,t')\mathrm{d}t'\mathrm{d}\mathbf{x}. \qquad (33)
\end{aligned}
$$

Algorithm 1. The Marchenko algorithm as implemented in the provided source code.

```
Main begin
    Reading SU-style input Data and Allocate arrays
    Initialization
    Ni(t) = f2p(t) = f1plus(t) = G_d(-t)
    f1min(t) = pmin(t) = 0.0
    for iter←0 to niter do
        synthesis(Refl, Ni, iRN)
        Ni(t)=−iRN(-t)
        pmin(t)+=iRN(t)
        applyMute(Ni, muteW)
        f2p(t) += Ni(t)
        else if (iter % 2 == 0) then
            f1min(t) −= Ni(-t)
        else
            f1plus(t) += Ni(t)
        end
    end
    Green(t) = pmin(t) + f2p(-t)
end
synthesis(Refl, Ni, iRN)
begin
    iRN = 0
    ∀ l, i: Fop(l,ω,i) = F {Ni(l,i,t)}
    for k←0 to nshots do
        #pragma omp parallel for
        for l←0 to Nfoc do
            for ω←ω_min to ω_max do
                sum(ω) = 0
                for i←0 to nrecv do
                    sum(ω) += Refl(k,ω,i) * Fop(l,ω,i)
                end
            end
            iRN(l,k,t) = F^-1 {sum(ω)}
        end
    end
end
```

In equation 33, the integration-convolution terms can be recognized as the summation of the unmuted N_i terms. By storing the sum of these unmuted terms of the integration-convolution (in p^-), the Green's functions can be calculated as a summation of previously computed values.

The program can compute the results of multiple focal points at the same time (*Nfoc* in Algorithm 1). This is convenient for calculating the Marchenko results (e.g., the Green's function) on a depth level or area of interest in one run. The computational advantage is that the reflection response has to be read in only once to compute the results of multiple focal points. The computations for different focal points are independent of each other. Hence, the code is OpenMP parallelized over the number of focal points (`Nfoc`).

The function `synthesis` in Algorithm 1 computes the integration-convolution, of the focusing update term N_i with R, in the frequency domain (the Fourier operator is denoted with $\mathcal{F}$). For the computation of only one focal point, loading the required input data into memory usually takes more time than the computational work. The implementation has additional functionality (not shown in Algorithm 1) to compute the upgoing and downgoing Green's functions in equations 2 and 3 and write intermediate computed fields (N_i) to disk.

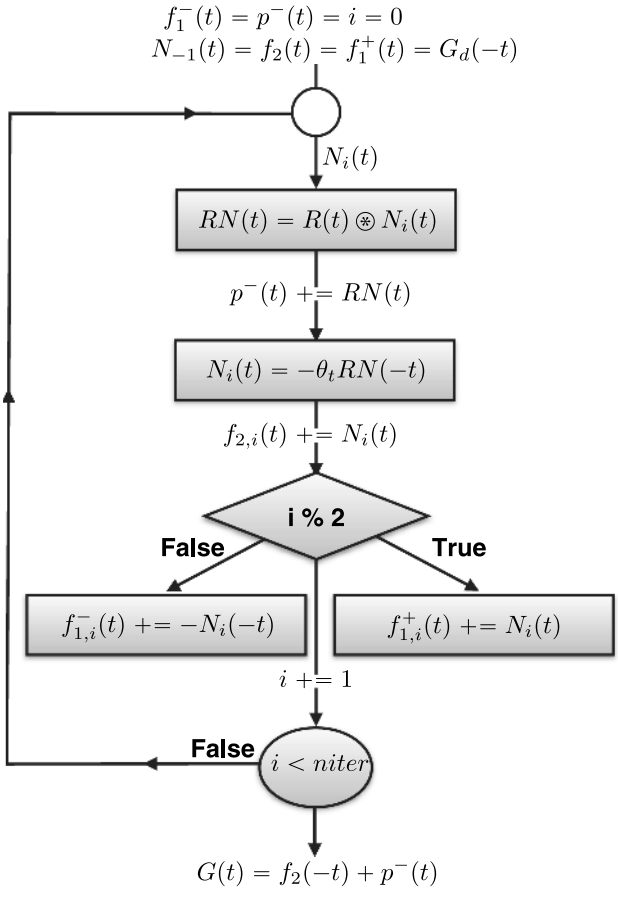

Figure 2. Flowchart of the Marchenko algorithm. In the notation, the lateral coordinates are omitted for a more compact notation. The symbol ⊛ represents the integration-convolution operator.

NUMERICAL EXAMPLES

To use the Marchenko method with numerically modeled data, it is very important that the amplitudes of the reflection response are correct. This is certainly also true for field data. Therefore, the importance of amplitude scaling is explained first before discussing the numerical examples in more detail.

In the summation of N_1 and G_d to compute $f_{1,1}^+$ in equation 20, it is important that the amplitude of the measured reflection data is accurate. A wrong amplitude of R will result in a wrong amplitude of $f_{1,1}^+$ and the scheme will not converge. This is illustrated with the following equations. Let us assume that we introduce a wrong scaling factor b in R to update $f_{1,i}^+$. Then, the first iterations will compute

$$\begin{aligned}
-bN_0(\mathbf{x}_R,\mathbf{x}_F,-t) &= \theta_t \int_{\partial\mathbb{D}_0}\int_{t'} bR(\mathbf{x}_R,\mathbf{x},t-t') \\
&\quad \times G_d(\mathbf{x},\mathbf{x}_F,-t')\mathrm{d}t'\mathrm{d}\mathbf{x}, \\
-b^2N_1(\mathbf{x}_R,\mathbf{x}_F,-t) &= \theta_t \int_{\partial\mathbb{D}_0}\int_{t'} bR(\mathbf{x}_R,\mathbf{x},t-t') \\
&\quad \times bN_0(\mathbf{x},\mathbf{x}_F,t')\mathrm{d}t'\mathrm{d}\mathbf{x}, \\
f_{1,1}^+(\mathbf{x}_R,\mathbf{x}_F,t) &= G_d(\mathbf{x}_R,\mathbf{x}_F,-t) + b^2N_1(\mathbf{x}_R,\mathbf{x}_F,t).
\end{aligned} \tag{34}$$

The update of $f_{1,1}^+$ involves an error of b^2 and in each next update of $f_{1,m}^+$ the error in the update N_{2m+1} will grow with b^{2m+2}. An incorrect amplitude in G_d is not a problem because the Marchenko equations are linear in the focusing function. An amplitude error can be factored out, and it does not change for higher iterations:

$$\begin{aligned}
-aN_0(\mathbf{x}_R,\mathbf{x}_F,-t) &= \theta_t \int_{\partial\mathbb{D}_0}\int_{t'} R(\mathbf{x}_R,\mathbf{x},t-t')aG_d(\mathbf{x},\mathbf{x}_F,-t')\mathrm{d}t'\mathrm{d}\mathbf{x}, \\
-aN_1(\mathbf{x}_R,\mathbf{x}_F,-t) &= \theta_t \int_{\partial\mathbb{D}_0}\int_{t'} R(\mathbf{x}_R,\mathbf{x},t-t')aN_0(\mathbf{x},\mathbf{x}_F,t')\mathrm{d}t'\mathrm{d}\mathbf{x}, \\
af_{1,1}^+(\mathbf{x}_R,\mathbf{x}_F,t) &= aG_d(\mathbf{x}_R,\mathbf{x}_F,-t) + aN_1(\mathbf{x}_R,\mathbf{x}_F,t).
\end{aligned} \tag{35}$$

Van der Neut et al. (2015c) introduces an adaptive amplitude-correction factor to correct for possible amplitude errors in R. By solving the Marchenko equation in an explicit series, the sensitivity of amplitude errors can be adjusted by adaptive subtraction of the focusing update terms. This approach makes it better suited to apply to field data (van der Neut et al., 2015a; Staring et al., 2016).

Brackenhoff (2016) and Thomsen (2016) develop estimation methodologies for a constant scaling factor b of R. These methods compensate for an overall amplitude mismatch in R, which is an important first step to apply the Marchenko method on measured data. Brackenhoff's method, for example, makes use of the fact that $G^-(\mathbf{x},\mathbf{x}_F,t)$ is identically zero for a point $\mathbf{x}_F$ below the deepest reflector.

The following will provide step-by-step directions how to compute the reflection response with accurate amplitudes:

- The reflection data must be deconvolved for the wavelet (Mildner et al., 2017). The result of this deconvolution is the reflection response of a zero-phase wavelet with a flat spectrum between the frequencies $f_{\min}$ and $f_{\max}$. Because we are computing the reflection response, we can avoid deconvolution and directly models the reflection response with

a source signature that has a flat frequency spectrum of amplitude 1.0:

$$s(t) = \int_{f_{\min}}^{f_{\max}} 1.0 \, \exp(-j2\pi f t) df. \tag{36}$$

The implemented flat wavelet spectrum has smooth transitions (a cosine taper) to the minimum, and from the maximum, frequency to avoid a very long wavelet in the time domain. The provided program `makewave` can generate these waveforms and the provided scripts give the `makewave` parameters used to calculate the source wavelet. Note: In the discrete implementation of the computation of the source wavelet in the frequency domain, one must not forget to multiply with the frequency interval Δf, when going from frequency to time with the Fourier transform. The source wavelet used in the examples is shown in Figure 3. A shift of 0.3 s (the parameter setting `t0=0.3` in `makewave`) is added to the source wavelet to make it causal and suitable to use in the finite-difference program. In the finite-difference modeling of the reflection response, the recording of the data is postponed with 0.3 s (parameter setting `rec_delay = 0.3` in `fdelmodc`) to set the peak of the wavelet back at the correct time.

- In the finite-difference program for modeling $R(\mathbf{x}_R, \mathbf{x}, t)$, an F_z source of vertical force is chosen (see the manual of the finite-difference modeling program `fdelmodc` for an explanation about the options). The receivers are placed at the same surface as the source and measure the pressure field.
- The amplitude scaling factor, in the finite-difference scheme for an F_z source with time signature $s(t)$, is defined in the update of particle velocity V_z as

$$V_z(x, z, t + \Delta t) = V_z(x, z, t) - \frac{\Delta P(x, z, t)}{\rho \Delta z} + \frac{\Delta t}{\rho \Delta x^2} s(t). \tag{37}$$

The discrete intervals $\Delta t, \Delta x = \Delta z$ are the steps in the finite-difference program, and ρ is the local density at the injection grid point of the source. The term $\Delta P/\Delta z$ is a fourth-order finite-difference implementation of the first derivative to z of pressure field P

- To compute R, from Green's functions calculated by the finite-difference program, only a factor of -2 is needed (equation 10 in Wapenaar et al., 2012). This factor -2 is included in the `marchenko` program when it reads in the reflection response R.
- The time convolution of R is implemented by a forward Fourier transformation from the time to the frequency domain, multiplication in the frequency domain, and back-transformation to the time domain. In the numerical implementation, the multiplication with Δt, for the convolution in time and with Δx for the integration over x, must be included as well. Together with the standard scaling factor of $1/N$ for discrete Fourier transformations when going from the time to the frequency domain and back to the time domain, with N the number of time samples, the scale factor to compute the time convolution and space integration in the frequency domain becomes

$$\frac{\Delta x \Delta t}{N}. \tag{38}$$

Building up the Green's function

The Marchenko algorithm is illustrated with a 2D horizontally layered model as shown in Figure 4. The numerical modeling is carried out with a finite-difference modeling program (Thorbecke and Draganov, 2011) that is also included in the software package. The input source signature used to model the reflection response $R(\mathbf{x}_R, \mathbf{x}, t)$ is approximately a sinc function with a flat spectrum of amplitude 1, as shown in Figure 3.

The full reflection matrix $R(\mathbf{x}_R, \mathbf{x}, t)$, for a fixed-spread geometry, can be constructed from one forward-modeled shot (Figure 4c) because the model contains no lateral variations. The constructed fixed-spread geometry ranges from -2250 to 2250 m with a 5 m distance between the source and receiver positions. The 5 m distance is chosen to avoid spatial aliasing. We use a laterally invariant medium because the time to compute the reflection response R in a laterally variant medium is too large to be practical for the desired reproducibility of the examples in this paper. However, the Marchenko method does not make any assumption about the medium and can handle lateral variations as well. Moreover, the demo directory

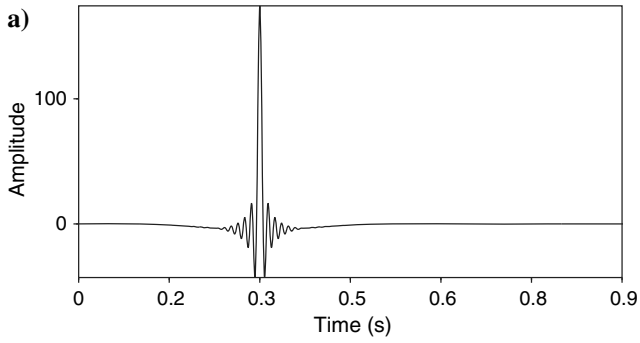

Source wavelet for modeling R.

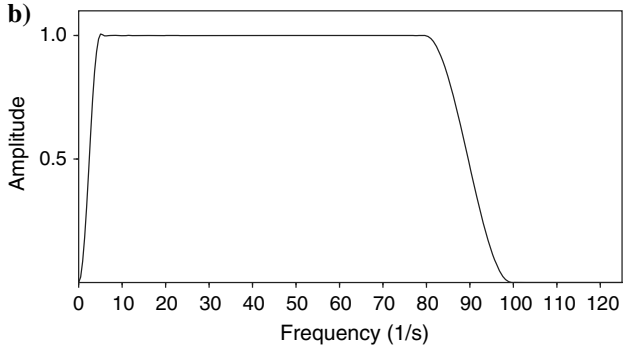

Amplitude spectrum of source wavelet.

Figure 3. Source wavelet with a flat frequency spectrum between $f_{\min}(= 5$ Hz) and $f_{\max}(= 80$ Hz) used to model the reflection response.

of the Marchenko program contains also an example with lateral variations in the model (`marchenko/demo/twoD`).

The transmission response, recorded at the surface for a source at a 900 m depth, is shown in Figure 4d. It has been modeled with a zero-phase Ricker source wavelet $s(t)$ that has its peak at 25 Hz. It is important that the chosen source wavelet to model G_d be zero phase; otherwise, the time reversals applied in the algorithm would not work properly and the Marchenko scheme would not converge. It is also preferable to choose a source wavelet that decreases rapidly in time. This is to minimize the occurrence of overlap between the direct arrival and the first reflections as is assumed in equation 11. In case of an overlap, the defined window function (θ_t in equation 12) cuts through the overlapping events, and the first reflection is not retrieved correctly.

The initialization step used to compute $f^-_{1,0}$ (equation 18) is illustrated in Figure 5. Each shot record in $R(\mathbf{x}_R, \mathbf{x}, t)$ is convolved with $G_d(\mathbf{x}_R, \mathbf{x}_F, -t)$, where $G_d(\mathbf{x}_R, \mathbf{x}_F, -t)$ shown in Figure 5 only contains the time reversal of the full transmission response as shown in Figure 4d. By making use of shift invariance $R(\mathbf{x}_R, \mathbf{x}, t) = R(\mathbf{x}_R - \mathbf{x}, 0, t)$, the time-convolution result is integrated (summed over all receiver positions $\mathbf{x}_R$) and results in one trace at the $\mathbf{x}$ position in the N_0 panel.

In $-N_0(\mathbf{x}, \mathbf{x}_F, -t)$, the dotted lines indicate the cutoff boundaries of the implemented time window $\theta(\mathbf{x}, \mathbf{x}_F, t)$. To suppress wrap-around events (from positive times wrapping to negative times), the time window $\theta(\mathbf{x}, \mathbf{x}_F, t)$, as introduced in equation 12, is symmetrized. Hence, from here onward $\theta(\mathbf{x}, \mathbf{x}_F, t)$ is zero for $t > t^\epsilon_d$ and $t < -t^\epsilon_d$, and unity for times inside $-t^\epsilon_d < t < t^\epsilon_d$. For deep focal points, one can also extend the time axis by padding zeros at the end of the array and in that way avoid the influence of wrap-around events in the time domain. In Appendix A, the treatment of time wrap-around is explained in more detail.

The events before the top dotted line and the events after the bottom dotted line are muted. The two remaining events originate from the two reflectors above the chosen focal point at a 900 m depth. A detailed explanation of the different events in the focusing functions is given by van der Neut et al. (2015b). Staring et al. (2016) give a similar explanation in case free-surface multiples are included in the Marchenko method. This initialization of f^-_1 is the input of the next step to compute a first estimate of f^+_1, given in equations 19 and 20.

The computation of $f^+_{1,1}$ involves the same time convolution and spatial integration operation, and it is illustrated in Figure 6. The result of the integration and convolution; $-N_1(\mathbf{x}, \mathbf{x}_F, -t)$ is, according to equation 20, time reversed, multiplied by -1 and added to $G_d(\mathbf{x}, \mathbf{x}_F, -t)$ to get the first estimate $f^+_{1,1}$. Note, that the lower (causal) part of the time window $\theta(\mathbf{x}, \mathbf{x}_F, t)$ mutes also the event at direct arrival time. This event at the direct arrival time t_d will end up in the update of the Green's function and will adjust the amplitude of the direct arrival in the Green's function (van der Neut et al., 2015b). This update of the direct arrival in the Green's function is explained in more detail below.

Figure 7 shows the results of the first four iterations of the Marchenko method. The first column represents the results of each convolution and integration of the focusing update term N_i with R. From these figure parts (all with the same clipping factor) one can observe that the amplitude of N_i becomes smaller with each next iteration.

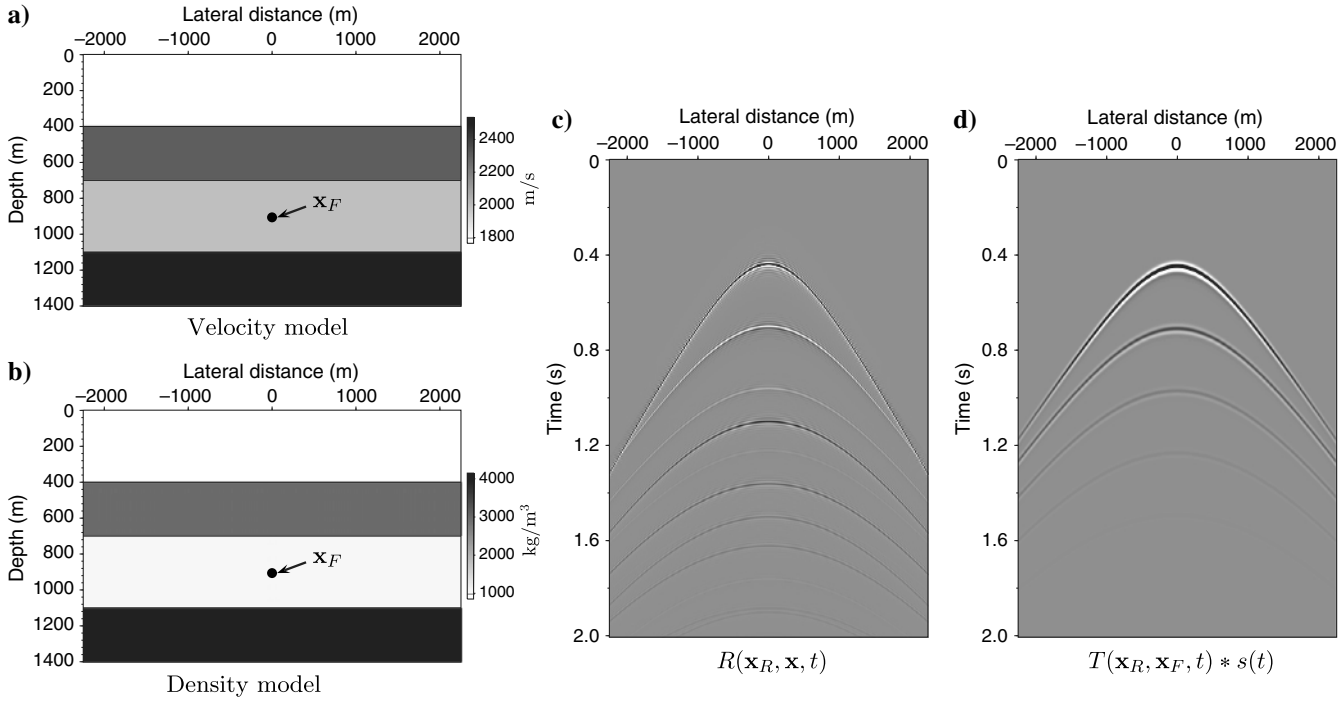

Figure 4. Four-layer model with (a) velocity and (b) density contrasts. (c) A shot record, with source position $\mathbf{x}(x = 0, z = 0)$ and receivers at $\mathbf{x}_R(x = x_r, z = 0)$, and (d) the transmission response from a source at $\mathbf{x}_F(x = 0, z = 900)$. Note that the source wavelet used to compute R (c) is given in Figure 3 and T (d) is modeled with a Ricker wavelet with a peak at 25 Hz.

The trace in the fifth column is a comparison between the reference Green's function (solid gray) and the computed Green's function (dotted black). In these traces, one can observe (indicated with arrows) that some events are weakened by subsequent iterations: The computed Green's function converges to the reference Green's function.

To get a better understanding of the computation of the Green's function, the first few iterations are discussed in more detail. The initialization of the method starts with G_d (equation 27), and G is computed according to equation 33. This gives

$$
\begin{aligned}
f_{2,0}(\mathbf{x}_F,\mathbf{x}_R,t) &= G_d(\mathbf{x}_R,\mathbf{x}_F,-t)\\
G_0(\mathbf{x}_R,\mathbf{x}_F,t) &= G_d(\mathbf{x}_R,\mathbf{x}_F,-t)\\
&+\int_{\partial\mathbb{D}_0}\int_{t'=-\infty}^{t} R(\mathbf{x}_R,\mathbf{x},t-t')\\
&\times G_d(\mathbf{x},\mathbf{x}_F,-t)\mathrm{d}t'\mathrm{d}\mathbf{x}+N_0(\mathbf{x}_R,\mathbf{x}_F,-t).
\end{aligned}
\tag{39}
$$

Note that in equation 39, the result of the first integration-convolution with R is **not** muted with θ_t. The initial estimate of Green's function is thus built up of three terms:

1) the direct arrival of the transmission response ($G_d(\mathbf{x}_R,\mathbf{x}_F,-t)$),
2) the integration-convolution of R with G_d, this is the (unmuted) top left panel in Figure 7, and
3) A θ_t muted and multiplied by -1 version of the integration-convolution of R with G_d: $N_0(\mathbf{x}_R,\mathbf{x}_F,-t)=-f_{1,0}^{-}(\mathbf{x}_R,\mathbf{x}_F,t)$, the second panel in the top row of Figure 7 multiplied by -1.

It is important to note that the result of the combination of the second and third terms just subtracts $f_{1,0}^{-}(t)$ (the events within the black-dotted lines) from the unmuted integration-convolution of R with G_d. This is the same as the inverse operation of the time window θ_t. To get the first estimate of the Green's function, $G_d(\mathbf{x}_R,\mathbf{x}_F,-t)$ is added to this result and gives the top-right panel in Figure 7. In the next iteration, we have

$$
\begin{aligned}
f_{2,1}(\mathbf{x}_F,\mathbf{x}_R,t) &= G_d(\mathbf{x}_F,\mathbf{x}_R,-t)+N_0(\mathbf{x}_F,\mathbf{x}_R,t)\\
G_1(\mathbf{x}_F,\mathbf{x}_R,t) &= G_0(\mathbf{x}_R,\mathbf{x}_F,t)\\
&+\int_{\partial\mathbb{D}_0}\int_{t'=-\infty}^{t} R(\mathbf{x}_R,\mathbf{x},t-t')\\
&\times N_0(\mathbf{x},\mathbf{x}_F,t)\mathrm{d}t'\mathrm{d}\mathbf{x}+N_1(\mathbf{x}_R,\mathbf{x}_F,-t).
\end{aligned}
\tag{40}
$$

Compared with the previous iteration, two new terms are added:

1) the integration-convolution of R with N_0, this is the (unmuted) left panel for $i=1$ in Figure 7 and
2) the θ_t muted, time reversed, multiplied by -1 version of the integration-convolution of R with N_0: $N_1(-t)$.

The combination of these two terms results in the subtraction of the events within the black-dotted lines from the unmuted integration-convolution of R with N_0.

Each next iteration follows this same pattern: The events within the time window θ_t (above t_d^e) are used to update the f_1 focusing

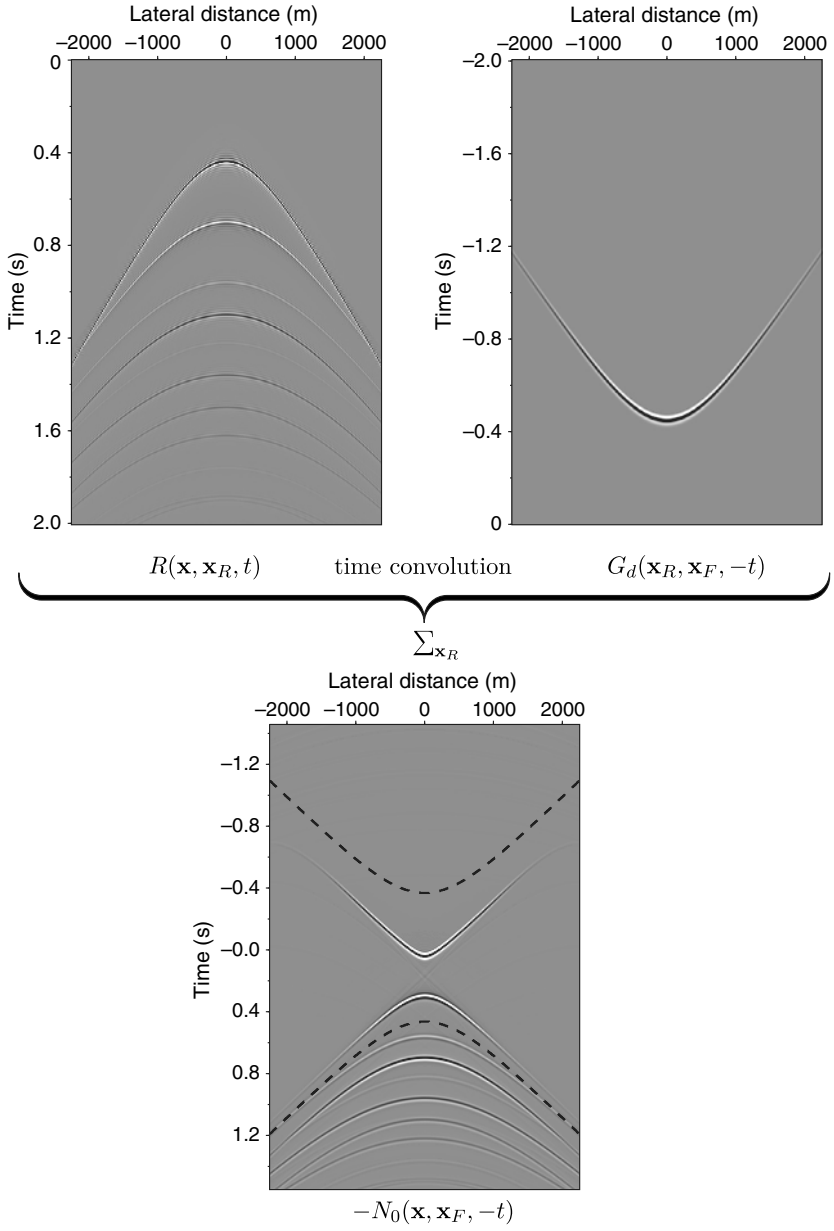

Figure 5. Initialization step to compute $f_{1,0}^{-}(\mathbf{x},\mathbf{x}_F,t)=-N_0(\mathbf{x},\mathbf{x}_F,-t)$. After applying the time window $\theta(\mathbf{x},\mathbf{x}_F,t)=\theta_t$ only events between the dotted lines remain in N_0. The mute window at $t<0$ is applied to mute the wrap-around events of the temporal convolution. This extra window at $t<0$ is only a practical solution and is not needed from the theory. Note the difference in the time axes of the three panels: positive for $R(t)$, negative for $G_d(-t)$, and negative and positive for $N_0(-t)$).

function, and the events outside the time window θ_t (below t_d^e) are used to update Green's function. Application of the window function θ_t separates the focusing function and the Green's function.

There is one important remark to make: The direct arrival T_d^{inv} in the focusing function f_1^+ is not updated, whereas the direct arrival G_d in the Green's function G is updated. In the first iteration (top row in Figure 7), the direct arrival in the Green's function G_0 is equal to G_d. In the second iteration shown in Figure 7, the amplitude of the direct arrival is corrected by the event in the unmuted $-N_1(-t)$ just below the black-dotted line of the mute window. This event in the unmuted $-N_1(-t)$ has an opposite sign to the direct arrival and decreases the amplitude of the direct arrival (van der Neut et al., 2015b). In the plotted trace of G_0, the amplitude of the direct arrival (the dotted line) is much higher than the reference (the gray line). In G_1, the amplitudes of the direct arrival between

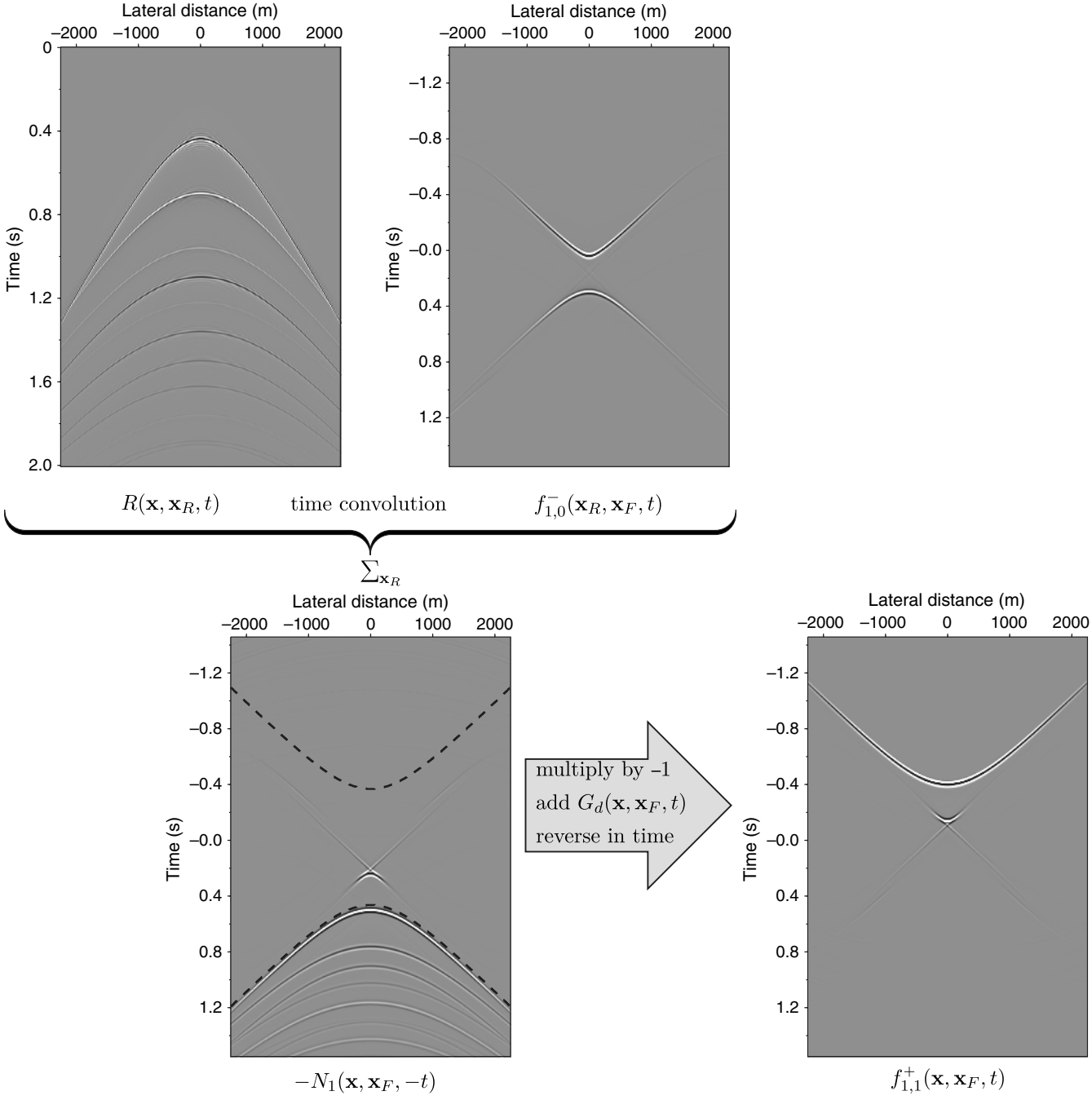

Figure 6. First iteration to compute $f_{1,1}^+(\mathbf{x}, \mathbf{x}_F, t)$ from $f_{1,0}^-(\mathbf{x}_R, \mathbf{x}_F, t)$. In the summation of G_d with N_1 it is important that the amplitudes of R are correct.

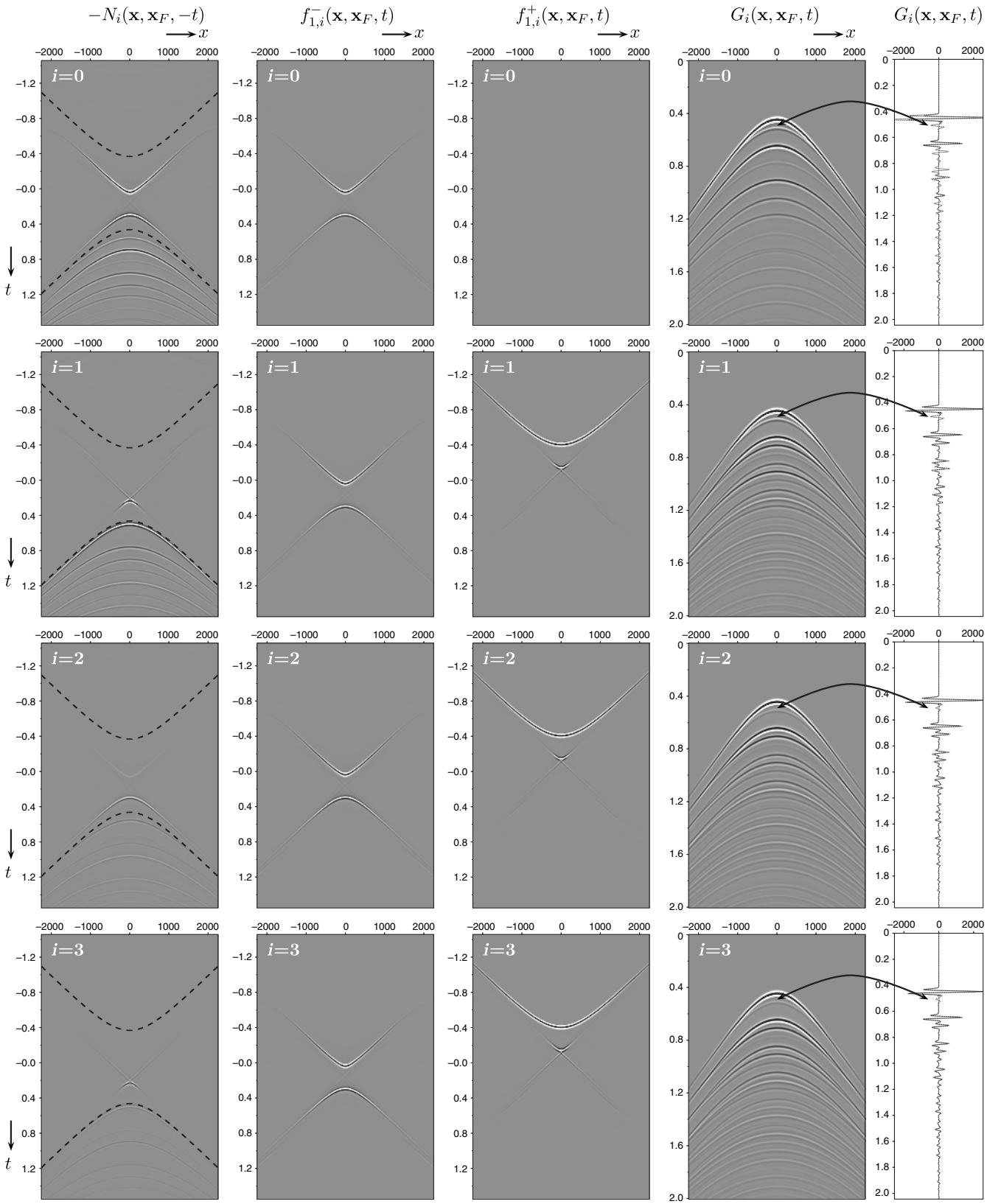

Figure 7. Four successive iterations of the Marchenko method. The arrows point to an event that does not belong to Green's function, and it is weakened at each iteration. The function $f^-_{1,i}$ (the second column) only changes from $i = 1$ to $i = 2$, whereas $f^+_{1,i}$ (the third column) changes from $i = 0$ to $i = 1$ and from $i = 2$ to $i = 3$. The clip level for N_i and G_i is the same for all panels. Labels of the horizontal and vertical axes are the same for all panels, and they are shown for the top and left panels.

reference and computed Green's function are already much closer. We do not expect that the scheme started with the approximation $T_d^{\text{inv}} \approx G_d$ will arrive at the correct amplitudes; to achieve accurate amplitudes, the inverse of the transmission transpose had to be used and not G_d. There is an offset-dependent scaling factor between the reference and the computed Green's function. Thorbecke et al. (2013) show that this estimate of the direct arrival does not have to be precise and can be based on a macromodel. The relative amplitudes between the events of the computed Green's function are correct and are shown in the trace comparison with the reference output in Figure 7.

The iterative corrections of the amplitude of Green's function are needed to take into account transmission losses. The result is that the upgoing field that arrives at $t = t_d$ has an amplitude that is equal to the local reflection coefficient of depth level z_f (Slob et al., 2014). In the next section, we will see how good this correction is when the f_2 focusing function is emitted into the medium.

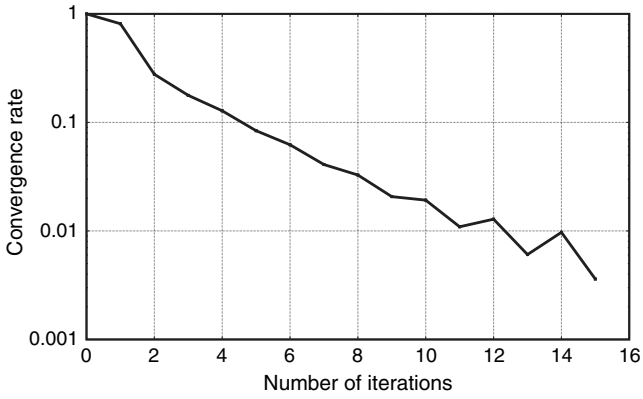

Figure 8. Logarithmic convergence rate of the marchenko/demo/oneD example for 16 iterations. The bumps at the end of the curve are caused by limited aperture artifacts. These artifacts are two orders of magnitude smaller than the main events.

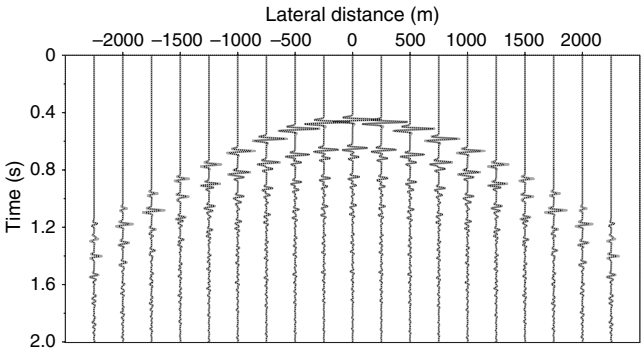

Figure 9. Comparison of the Marchenko computed Green's function after eight iterations with the reference Green's function: The solid-gray trace in the background is the reference, and the dotted-black trace is the Green's function computed with the Marchenko method.

Broggini et al. (2014) use the energy before the direct arrival in Green's function to define the convergence of the scheme. In the provided Marchenko program, there is no stopping criteria built in, to give the user the freedom to choose the number of iterations carried out. The energy in the focusing update term $(\sqrt{\sum_{x,t} N_i^2(x,t)})$ is computed and printed for each iteration and can be monitored for convergence. In each next iteration, this energy should become smaller. The convergence rate for eight iterations is shown in Figure 8.

A comparison with the reference Green's function and the Marchenko-computed Green's function after eight iterations is shown in Figure 9. The difference with the reference Green's function is negligible in the middle part of the picture around $x = 0$. A small amplitude mismatch increases slightly with the increasing offset. Closer to the edge of the acquisition (±2250 m), the difference with the reference becomes larger because the full Fresnel zone is not included in the acquisition. The higher wavenumbers, more present at earlier times, are also not captured by the limited acquisition. Note that after approximately 1.5 s, the presence of higher wavenumbers becomes smaller, and the amplitude error at the far offsets also decreases. To suppress artifacts from limited acquisition aperture, tapers can be applied to the edges of the initial focusing operator and/or the reflection response. In our experience, these tapers have limited effects on suppressing these artifacts. Depending on the specific events at the boundaries of the model the finite aperture effect could slightly be attenuated. In some cases, the taper shifts the problem to the nontapered part adjacent to the tapered region and finite aperture artifacts remain. Another, usually smaller, amplitude mismatch is caused by the use of the time reversal of the direct arrival in the transmission response G_d (equation 11) instead of the inverse.

Propagating the focusing function

One of the properties of the defined $f_2(\mathbf{x}_F, \mathbf{x}, t)$ focusing function in equation 6 is that it will focus at $t = 0$ at the focal point $\mathbf{x}_F$. This property can be demonstrated by emitting $f_2(\mathbf{x}_F, \mathbf{x}, t)$ from $\partial\mathbb{D}_0$ into the medium and show that it has a focus at position $\mathbf{x}_F$ at snapshot $t = 0$ (Singh et al., 2016; Wapenaar et al., 2017). If the transmission losses in the events in f_2 have correctly been taken into account, then all internal multiples will be canceled at (and only at) $t = 0$. The left column of Figure 10 shows five snapshots at times -0.30, -0.15, -0.03, -0.02, and 0.0. The snapshot at $t = 0$ indeed shows only a focus at the focal point. In the snapshots at times $t = -0.03$ and $t = -0.02$, it is observed that events related to internal multiples have opposite amplitude and travel toward each other to cancel out at $t = 0$.

The second column of Figure 10 shows snapshots at positive times, after the wavefield has focused at $t = 0$. After $t = 0$, the focused and dimmed events separate again and continue their path.

Adding the snapshots at negative times to the corresponding snapshots at positive times defines the snapshots of the homogeneous Green's function (Wapenaar et al., 2016) with a virtual source at $\mathbf{x}_F$. The third column in Figure 10 shows these combined snapshots, in which the snapshots at positive and negative times are summed, and they represent the causal part of the homogeneous Green's function. These snapshots can be interpreted as the response of a virtual source located at the position of the focal point $\mathbf{x}_F$.

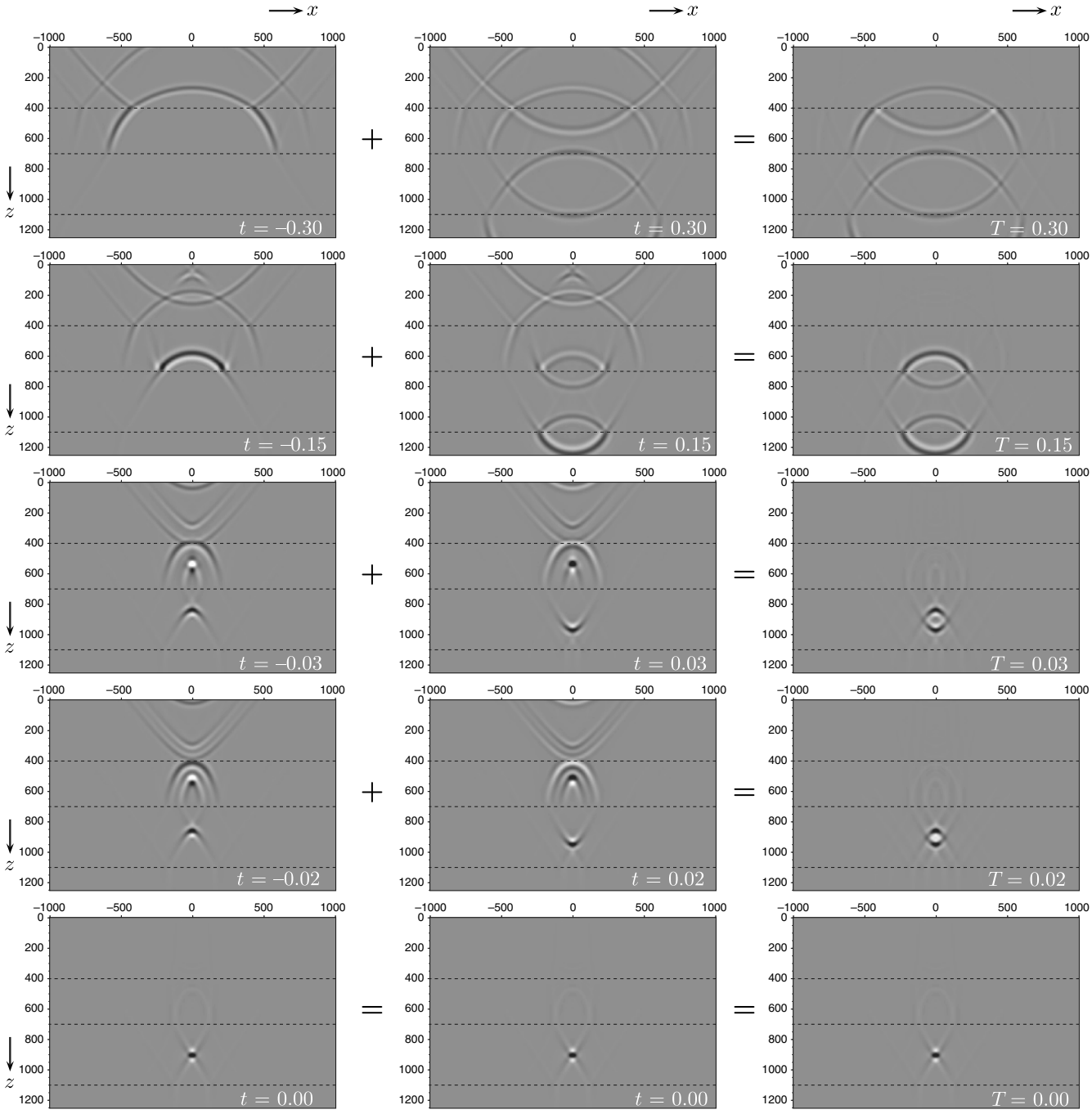

Figure 10. Snapshots of propagation of focusing function f_2 through the actual medium. The left column shows snapshots at acausal times, and the middle column shows snapshots at causal times. The rightmost column shows the addition of the acausal snapshots at negative times with the corresponding causal snapshots at positive times (time T). Labels of the horizontal and vertical axes are the same for all panels, and they are shown for the top and left panels.

CONCLUSION

The iterative Marchenko method computes focusing functions which in turn can be used to compute upgoing and downgoing Green's functions from a virtual source position in the subsurface. For the method to converge, the amplitudes of the (modeled) reflection response must be deconvolved for the source signature and correctly scaled. In each iteration, a time convolution and spatial integration is carried out between a focusing-update term N_i and the reflection data. The result of this integration is split by a time window that is defined by the first-arrival time from the virtual source position. The events before the first arrival define at each iteration a new N_i, which is used in the next iteration. The events after the time window update the Green's function. The main com-

putational work in each iteration is the computation of these focusing-update terms N_i. The focusing functions are updated by adding the computed N_i terms.

ACKNOWLEDGMENTS

We are grateful for the many constructive comments and suggestions that we received from C. A. da Costa Filho, two anonymous reviewers, and the associate editor F. Brogginni. The reviewers helped to improve the readability of the paper and also made it better suited for an introduction to the Marchenko method.

APPENDIX A

INPUT PARAMETERS AND IMPLEMENTATION DETAILS

The provided marchenko source-code package contains two main programs:

- `fmute`: picks the first-arrival time from a transmission response and mutes along this time
- `marchenko`: solves for the focusing functions in the Marchenko method and computes the Green's functions.

The `fmute` program tracks the first arrival from a transmission response to a focal point in the subsurface. Its main use is to separate the direct arrival of the transmission response (G_d) from the multiple scattering coda (M^+), a similar separation to that presented in equation 11. In the examples provided, the transmission response is also computed by finite-difference modeling and the direct arrival needs to be separated from the coda. For example, `fmute` is used to compute $G_d(t)$ in Figure 5 from $T(t)$ in Figure 4d. The program `fmute` is not needed if a method is used (e.g., an eikonal solver) that computes the direct arrival in a direct way. The output G_d of the `fmute` program is the input `file_inv` of the `marchenko` program. The different parameters of fmute are shown in the self-documentation of the program:

```
fmute - mute in time domain file_shot along curve of maximum amplitude in file_mute
fmute file_shot= file_mute= [optional parameters]
Required parameters:
  file_mute= ......input file with event that
                   defines the mute line
  file_shot= ......input data that are muted
Optional parameters:
  file_out=........output file
  above=0 ... ..... mute after(0), before(1) or
                   around(2) the maximum times
                   of file_mute ..... options
                   4 is the inverse of 0, and
                   -1 is the inverse of 1
  shift=0 ... ..... number of points above(pos-
                   itive) / below(negative)
                   maximum time for mute
  check=0 ......... plots muting window on top
                   of file_mute: output file
                   check.su
  scale=0  ........scale data by dividing
                   through the maximum
  hw=15 ...........number of time samples to
                   look up and down in the next
                   trace for the maximum
  smooth=0 ........number of points to smooth
                   the mute with a cosine
                   window
  verbose=0....... silent option; >0 display
                   info
```

If `file_mute` is not provided, `file_shot` will be used instead to pick the first-arrival times.

The `above` option is explained in Figure A-1 and separates in different ways the direct arrival time (t_d) from the coda. The `above=0` and `above=4` options have also a truncation point at the lower end of the time axis, with the time reversal of t_d, to mute wrap-around events introduced by the periodicity of the discrete Fourier transform. Note that the lower end of the time axis can also represent negative times. The `above=2` option defines a passing window around t_d, and it is convenient to select the direct arrival of the transmission response in case the first arrival also contains head waves.

To find the first-arrival time in `file_mute`, a simple tracking algorithm is implemented. At the trace position equal to the source

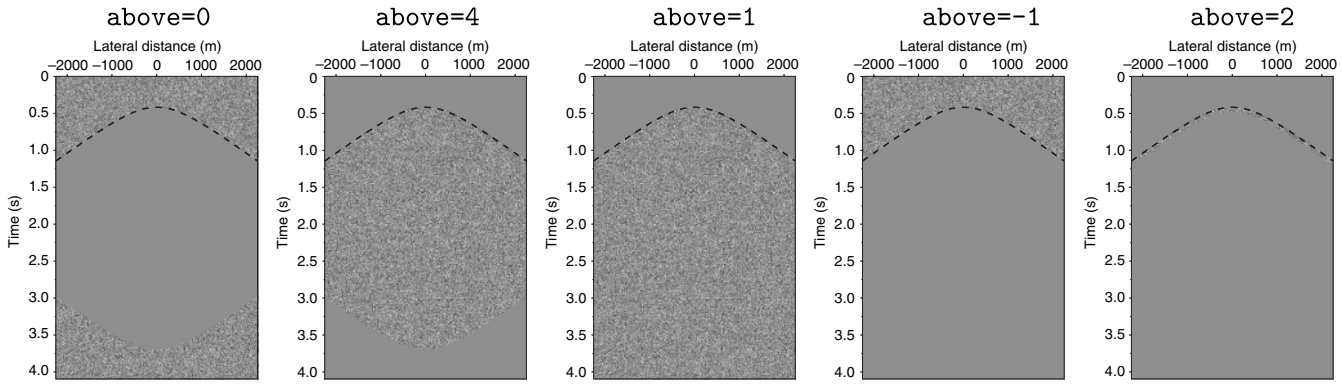

Figure A-1. The different options of the above parameter in the fmute and marchenko programs, illustrated with a shot panel consisting of noise.

position, the algorithm searches for the maximum value in that trace. It is assumed that this is the first-arrival time at the source position. For complex models, this might not be true, and it is therefore always good to enable `check=1` and verify in the created output file `check.su` if the program has tracked the correct direct arrival time. Starting at the time-sample position of the maximum ($j_{\max}$) in the source trace i, the algorithm looks in neighboring traces ($i \pm 1$) for the maximum. It only searches for this maximum in a restricted time window. For example, the maximum in the left trace is searched in the time window $j_{\max} - \mathrm{hw} < t_{i-1} < j_{\max} + \mathrm{hw}$, where `hw` is several samples given as the input parameter. If there are head waves present, the search algorithm can lose track of the direct arrival, so it is good practice to choose a small `hw` (four to eight samples).

The `shift` option represents the ε in t_d^{ε}, and it is needed to include the width of the wavelet in the mute window. Figure A-2 shows the effect of setting a negative or positive shift to exclude or include the width of the wavelet. With the `above=-1` option, a positive shift will mute the direct arrival, whereas a negative shift will preserve the direct arrival.

The parameter `smooth` defines a transition zone (in samples) going from one to zero in the mute window. Using a few time samples (3–5) for the smooth transition zone is enough to give satisfactory results. The direction of the taper, going from zero to one, is away from $\pm t_d$.

The `marchenko` program has the following parameters and options:

```
MARCHENKO - Iterative Green's function and focusing functions retrieval
 marchenko file_tinv= file_shot= [optional parameters]
 Required parameters:
   file_tinv= ..... direct arrival from focal
                    point: G_d
   file_shot= ..... Reflection response: R
 Optional parameters:
 INTEGRATION
   tap=0 ........... lateral taper focusing(1),
                    shot(2) or both(3)
   ntap=0 .......... number of taper points at
                    the boundaries
   fmin=0 .......... minimum frequency in the
                    Fourier transform
   fmax=70 ......... maximum frequency in the
                    Fourier transform
 MARCHENKO ITERATIONS
   niter=10 ........ number of iterations
 MUTE-WINDOW
   above=0 ......... mute above(1), around(0) or
                    below(-1) the first travel-
                    times of file_tinv
   shift=12 ........ number of points above(pos-
                    itive) / below(negative)
                    traveltime for mute
   hw=8 ............ window in time samples to
                    look for the maximum in
                    the next trace
   smooth=5 ........ number of points to smooth
                    mute with the cosine window
 REFLECTION RESPONSE CORRECTION
   tsq=0.0 ........ scale factor n for t^n for
                    true amplitude recovery
   scale=2 ........ scale factor of R for summa-
                    tion of Ni with G_d
   pad=0 ........... amount of samples to pad the
                    reflection series
 OUTPUT DEFINITION
   file_green=..... output file with the full
                    Green's function(s)
   file_gplus= ..... output file with G+
   file_gmin= ...... output file with G-
   file_f1plus= .... output file with f1+
   file_f1min= ..... output file with f1-
   file_f2= ........ output file with f2 (=p+)
   file_pplus= ..... output file with p+
   file_pmin= ..... output file with p-
   file_iter= ..... output file with -Ni(-t) for
                    each iteration
   verbose=0 ..... silent option; >0 displays
                    info.
```

The number of iterations required for convergence depends on the reflection strengths and number of events in the model; a complex model will need more iterations. Typically, the number of iterations is between 8 and 20. An automatic stopping criterion could be based on the energy in the focusing update N_i. This stopping criterion is not implemented to give the user the freedom to choose the number of iterations.

To suppress artifacts from a limited acquisition aperture, tapers can be applied to the edges of the initial focusing operator (`tap=1`) and/or the reflection response (`tap=2`). In our experience, these tapers have limited effects on suppressing the finite-acquisition-

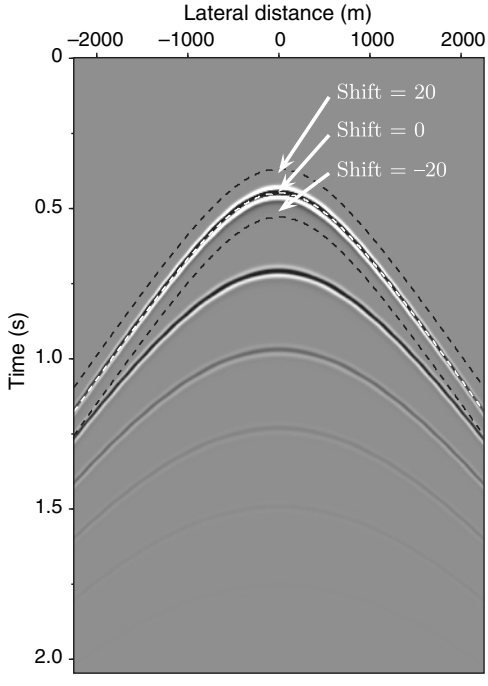

Figure A-2. The shift parameter in the fmute and marchenko programs.

related artifacts and tapering is usually not enabled. The mute-window parameters have the same meaning as in the `fmute` program.

The temporal convolution of events at positive times in the focusing update term causes events in R to be shifted forward in time. Events at negative times will shift events in R backward in time. In the Marchenko method, it is important that these backward-shifted events are properly handled. For deeper focal points, some events can be shifted to negative times; see, for example, N_0 in Figure 5. By implementing the temporal convolution in the frequency domain, we make use of the periodic property of the discrete Fourier transformation: Negative times wrap around to the end of the discrete time axis.

The reason to symmetrize the time window θ_t is to suppress unwanted time wrap-around effects. The time-wrap-around effects can also be avoided by padding zeros to the time traces in R, making the time traces `2*nt` long, where the last `nt` samples are zeros. The parameter pad will `pad` zeros to the time traces of R. Adding extra time samples will lead to longer computation times. Therefore, we prefer to use a symmetrized time window to suppress the unwanted effects of time wrap around.

The `scale` parameter can be useful when the modeled data do not have the correct amplitude, and it represents the previously mentioned b scaling factor of the reflection response. The program can optionally, when the file-names `file_*` are defined, output results of computed Green's and focusing functions. Defining `file_iter` writes for each iteration the focusing update term $-N_i(-t)$ (=iRN(t) in Algorithm 1) before applying the mute window. By setting the verbose option to 2, the energy of the focusing update term is printed out for each iteration and can be used to monitor the convergence of the scheme.

The code to reproduce all figures in this paper can be found in the directory `marchenko/demo/oneD`. The README file in that directory explains in detail how to run the scripts. A more complicated (laterally varying) model can be found in the directory marchenko/demo/twoD. This example usually takes several hours to complete the reflection data modeling on a personal computer, and it is thus not discussed.

In addition to the Marchenko programs, the package also contains the previously published finite-difference modeling code, which is used to model all data in the examples, in directory `fdelmodc` (Thorbecke and Draganov, 2011). The directory `utils` contains programs to calculate a gridded model (`makemod`), source wavelets (`makewave`), and programs for basic processing steps.

REFERENCES

Behura, J., K. Wapenaar, and R. Snieder, 2014, Autofocus imaging: Image reconstruction based on inverse scattering theory: Geophysics, **79**, no. 3, A19–A26, doi: 10.1190/geo2013-0398.1.

Brackenhoff, J., 2016, Rescaling of incorrect source strength using Marchenko Redatuming: M.Sc. thesis, TU Delft Repository, Delft University of Technology, http://resolver.tudelft.nl/uuid:0f0ce3d0-088f-4306-b884-12054c39d5da, accessed 31 August 2016.

Broggini, F., and R. Snieder, 2012, Connection of scattering principles: A visual and mathematical tour: European Journal of Physics, **33**, 593–613, doi: 10.1088/0143-0807/33/3/593.

Broggini, F., R. Snieder, and K. Wapenaar, 2012, Focusing the wavefield inside an unknown 1D medium: Beyond seismic interferometry: Geophysics, **77**, no. 5, A25–A28, doi: 10.1190/geo2012-0060.1.

Broggini, F., K. Wapenaar, J. van der Neut, and R. Snieder, 2014, Data-driven Green's function retrieval and application to imaging with multidimensional deconvolution: Journal of Geophysical Research: Solid Earth, **119**, 425–441, doi: 10.1002/2013JB010544.

Cohen, J. K., and J. W. Stockwell, 2016, CWP/SU: Seismic Un*x Release No. 43R4: An open source software package for seismic research and processing: Center for Wave Phenomena, Colorado School of Mines.

da Costa Filho, C. A., G. A. Meles, and A. Curtis, 2017, Elastic internal multiple analysis and attenuation using Marchenko and interferometric methods: Geophysics, **82**, no. 2, Q1–Q12, doi: 10.1190/geo2016-0162.1.

da Costa Filho, C. A., M. Ravasi, and A. Curtis, 2015, Elastic P- and S-wave autofocus imaging with primaries and internal multiples: Geophysics, **80**, no. 5, S187–S202, doi: 10.1190/geo2014-0512.1.

da Costa Filho, C. A., M. Ravasi, A. Curtis, and G. A. Meles, 2014, Elastodynamic Green's function retrieval through single-sided Marchenko inverse scattering: Physical Review E, **90**, 063201.

Meles, G. A., K. Löer, M. Ravasi, A. Curtis, and C. A. da Costa Filho, 2015, Internal multiple prediction and removal using Marchenko autofocusing and seismic interferometry: Geophysics, **80**, no. 1, A7–A11, doi: 10.1190/geo2014-0408.1.

Meles, G. A., K. Wapenaar, and A. Curtis, 2016, Reconstructing the primary reflections in seismic data by Marchenko redatuming and convolutional interferometry: Geophysics, **81**, no. 2, Q15–Q26, doi: 10.1190/geo2015-0377.1.

Mildner, C., F. Broggini, K. de Vos, and J. O. A. Robertsson, 2017, Source wavelet amplitude spectrum estimation using Marchenko Focusing Functions: 79th Annual International Conference and Exhibition, EAGE, Extended Abstracts, We B2 01.

Ravasi, M., I. Vasconcelos, A. Kritski, A. Curtis, C. A. da Costa Filho, and G. A. Meles, 2016, Target-oriented Marchenko imaging of a North Sea field: Geophysical Journal International, **205**, 99–104, doi: 10.1093/gji/ggv528.

Singh, S., R. Snieder, J. Behura, J. van der Neut, K. Wapenaar, and E. Slob, 2015, Marchenko imaging: Imaging with primaries, internal multiples, and free-surface multiples: Geophysics, **80**, no. 5, S165–S174, doi: 10.1190/geo2014-0494.1.

Singh, S., J. van der Neut, K. Wapenaar, and R. Snieder, 2016, Beyond Marchenko — Obtaining virtual receivers and virtual sources in the subsurface: 86th Annual International Meeting, SEG, Expanded Abstracts, 5166–5171.

Slob, E., 2016, Green's function retrieval and Marchenko imaging in a dissipative acoustic medium: Physical Review Letters, **116**, 164301, doi: 10.1103/PhysRevLett.116.164301.

Slob, E., and K. Wapenaar, 2017, Theory for Marchenko imaging of marine seismic data with free surface multiple elimination: 79th Annual International Conference and Exhibition, EAGE, Extended Abstracts, Tu A1 04.

Slob, E., K. Wapenaar, F. Broggini, and R. Snieder, 2014, Seismic reflector imaging using internal multiples with Marchenko-type equations: Geophysics, **79**, no. 2, S63–S76, doi: 10.1190/geo2013-0095.1.

Staring, M., R. Pereira, H. Douma, J. van der Neut, and K. Wapenaar, 2017, Adaptive double-focusing method for source-receiver Marchenko redatuming on field data: 87th Annual International Meeting, SEG, Expanded Abstracts, 4808–4812.

Staring, M., J. van der Neut, and K. Wapenaar, 2016, An interferometric interpretation of Marchenko redatuming including free-surface multiples: 86th Annual International Meeting, SEG, Expanded Abstracts, 5172–5176.

Thomsen, H., 2016, Investigating the robustness of Green's function retrieval via Marchenko focusing and Seismic Interferometry: M.Sc. Thesis, ETH Zürich.

Thorbecke, J., 2017, GitHub repository of Source code, https://github.com/JanThorbecke/OpenSource.

Thorbecke, J., and D. Draganov, 2011, Finite-difference modeling experiments for seismic interferometry: Geophysics, **76**, no. 6, H1–H18, doi: 10.1190/geo2010-0039.1.

Thorbecke, J., J. van der Neut, and K. Wapenaar, 2013, Green's function retrieval with Marchenko equations: A sensitivity analysis: 83rd Annual International Meeting, SEG, Expanded Abstracts, 3888–3893.

van der Neut, J., J. Thorbecke, K. Wapenaar, and E. Slob, 2015a, Inversion of the multidimensional Marchenko equation: 77th Annual International Conference and Exhibition, EAGE, Extended Abstracts, We N106 04.

van der Neut, J., I. Vasconcelos, and K. Wapenaar, 2015b, On Green's function retrieval by iterative substitution of the coupled Marchenko equations: Geophysical Journal International, **203**, 792–813, doi: 10.1093/gji/ggv330.

van der Neut, J., and K. Wapenaar, 2016, Adaptive overburden elimination with the multidimensional Marchenko equation: Geophysics, **81**, no. 5, T265–T284, doi: 10.1190/geo2016-0024.1.

van der Neut, J., K. Wapenaar, J. Thorbecke, E. Slob, and I. Vasconcelos, 2015c, An illustration of adaptive Marchenko imaging: The Leading Edge, **34**, 818–822, doi: 10.1190/tle34070818.1.

Vasconcelos, I., K. Wapenaar, J. van der Neut, C. Thomson, and M. Ravasi, 2015, Using inverse transmission matrices for Marchenko redatuming in highly complex media: 85th Annual International Meeting, SEG, Expanded Abstracts, 5081–5086.

Wapenaar, K., F. Broggini, E. Slob, and R. Snieder, 2013, Three-dimensional single-sided Marchenko inverse scattering, data-driven focusing, Green's function retrieval, and their mutual relations: Physical Review Letters, **110**, 084301, doi: 10.1103/PhysRevLett.110.084301.

Wapenaar, K., F. Broggini, and R. Snieder, 2012, Creating a virtual source inside a medium from reflection data: Heuristic derivation and stationary-phase analysis: Geophysical Journal International, **190**, 1020–1024.

Wapenaar, K., and E. Slob, 2014, On the Marchenko equation for multicomponent single-sided reflection data: Geophysical Journal International, **199**, 1367–1371, doi: 10.1093/gji/ggu313.

Wapenaar, K., J. Thorbecke, and J. van der Neut, 2016, A single-sided homogeneous Green's function representation for holographic imaging, inverse scattering, time-reversal acoustics and interferometric Green's function retrieval: Geophysical Journal International, **205**, 531–535, doi: 10.1093/gji/ggw023.

Wapenaar, K., J. Thorbecke, J. van der Neut, F. Broggini, E. Slob, and R. Snieder, 2014a, Green's function retrieval from reflection data, in absence of a receiver at the virtual source position: The Journal of the Acoustical Society of America, **135**, 2847–2861, doi: 10.1121/1.4869083.

Wapenaar, K., J. Thorbecke, J. van der Neut, F. Broggini, E. Slob, and R. Snieder, 2014b, Marchenko imaging: Geophysics, **79**, no. 3, WA39–WA57, doi: 10.1190/geo2013-0302.1.

Wapenaar, K., J. Thorbecke, J. van der Neut, E. Slob, and R. Snieder, 2017, Virtual sources and their responses, Part II: Data-driven single-sided focusing: Geophysical Prospecting, doi: 10.1111/1365-2478.12495.